International Conference on More Electric Aircraft (MEA2021), 20-21 October, Bordeaux, France
URL:https://see.asso.fr/369398_mea2021-proceedings/

Designing Low-weight Switched Reluctance Motors for Electric Multirotor Propulsion System

Marcin Biczyski (1), Rabia Sehab (2), Guillaume Krebs (3), James F. Whidborne (1), Patrick Luk (1)
1: Cranfield University, MK43 0AL Cranfield, UK – m.biczyski@cranfield.ac.uk
2: ESTACA Campus West, Laval, France
3: Group of electrical engineering - Paris, CNRS, CentraleSupélec, Paris-Saclay Univ., Sorbonne Univ., France

Abstract

One of the ways in which we can facilitate the introduction of UAVs, especially autonomous ones, into public airspaces is to increase their safety. Brushless DC motors used for the majority of RC vehicles have multiple vulnerabilities, most of which connected with the reliance on neodymium magnets. To reduce the number of possible points of failure, switched reluctance motor technology is researched as an alternative, because of reliability, robustness and the lack of rare earth materials. To take advantage of these features, a motor design optimization process was adopted, which uses 2D FEM models. These do not capture certain 3D effects, such as end-winding inductance, what has led to considerable decrease in performance when used in a multirotor propulsion chain. The presented approach keeps the 2D-based optimization approach and focuses on improving the performance as a next step in the design process. Four methods are evaluated – two of them aiming at improving the motor's flux network and two focused on increasing the voltage. Taking into consideration the application, the methods are assessed not only based on performance improvement, but also on predicted platform weight change and price increase.

Introduction

Recent advances in electric motor technology have driven the development of novel air vehicle configurations, particularly multirotors. These excel in the 1-10 kg weight range, where they operate as unmanned vehicles, and as such, are excellent candidates for development of autonomous technologies. Even in higher weight ranges these have received a lot of interest, especially in the Urban Air Mobility market. However, this type of configuration is heavily limited by its weight, as most of the lift produced comes from propeller thrust. What is more, in order to fully utilize their potential, these vehicles must be extremely reliable, particularly for operation in close proximity to humans (e.g. package delivery, air taxi).

The Brushless Direct Current (BLDC) motors mounted on most currently available Unmanned Aerial Vehicles (UAVs), have a good power to weight ratio, but leave a lot to be desired in terms of reliability. Their dependence on neodymium magnets to create a rotating magnetic field is a disadvantage during faults, as even an unpowered motor still generates back-EMF due to rotor and propeller inertia, which can generate faults in other parts of the system [1]. Even in healthy operation, the magnets are a risk factor due to high operational temperatures or overcurrent, shortening their lifespan or even leading to complete demagnetization [2].

A potential solution lies with Switched Reluctance (SR) motors. These machines are doubly salient with teeth on both stator and rotor, which eliminates the need for additional magnetic field from magnets (although it is possible to integrate these as well). A disadvantage is their higher weight (although alternative topologies exist, that partially address this issue), but the possible increase in reliability might provide a worthy tradeoff. SR motors were not popular until recent years due to the high computing power required for accurate control, but nowadays they are finding their way into the electric vehicle industry with considerable success [3].

To test the feasibility of SR motors for multirotor UAV propulsion, a demonstrator quadrotor drone is to be outfitted with four SR-based actuating chains, as illustrated in Fig. 1. This paper will describe the design of SR motors and the verification steps that were taken to ensure the motors met the performance specifications with minimum weight.

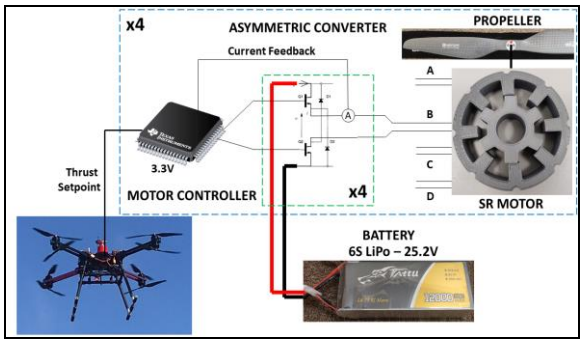

Fig. 1: Actuation chain schematic of the demonstrator drone

SR motor design

The SR motor design process started with a set of specifications for different drone MTOWs, using part of the procedure described in [4]. Complimentary motor designs (based on a conventional topology) were optimized using a MATLAB implementation of the DIRECT algorithm [5], along with MRVsim

software [6] to compute the flux network and simulate the performance at rated speed. The optimization objective is to achieve specified torque under weight and current density constraints. The outline of the methodology is shown in Fig. 2 and the design details of the optimized motor are listed in Table 1. Due to the propeller load increasing with speed, only the rated parameters are taken into consideration.

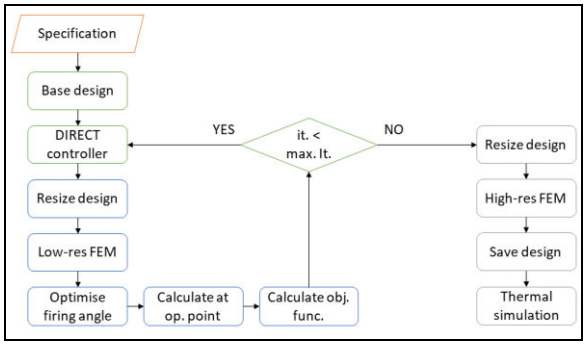

Fig. 2: SR motor for UAV applications optimization methodology

A possible drawback of this approach is that it is based on 2D FEM motor models, but in industrial, commercial aviation or EV applications these models give results close enough to the measured data [7]. UAVs, however, require much smaller machines. In this study, for a 10 kg quadrotor an SR motor was designed with 71 mm stator outer diameter and only 15 mm stack length. In such machines, the effects of end-winding inductance or flux leakage in 3rd dimension have much more impact. This results in an estimated 0.15 mH increase in the unaligned and 0.05 mH increase in the aligned unsaturated region of the flux network, as shown in Fig. 3.

Mitigation strategies

In SR machines, the driving torque comes from the change of flux linkage with time and with rotor position. This can be approximated (not considering saturation) with equations adapted from [8]:

$$vi = Ri^2 + Li\frac{di}{dt} + \omega_m i^2 \frac{dL}{dt} \quad (1)$$

$$T_e = \frac{1}{2} i^2 \frac{dL}{d\theta} \quad (2)$$

where v is voltage, i is current, R is winding resistance, L is winding self-inductance, ω_m is rotor speed, T_e is instantaneous torque and θ is rotor position.

Therefore, the average torque over one motor stroke (one phase energization) is proportional to the area between the two curves, and as is clear from Fig. 3, that has decreased between the 2D and 3D models. Therefore, one way to return motor performance to the expected level is to increase this area, by either increasing the saturation level or by improving the magnetic flux density in the teeth.

Parameter	*Original design*
Number of phases	4
Stator teeth	8
Rotor teeth	6
Phase resistance	0.11 Ohm
Voltage	22.2 V
Power	640 W
Rated torque	1.10 Nm
Rated speed	5508 RPM
Rated phase current	23 A r.m.s.
Rated efficiency	73%

Table 1: Parameters of the optimised SR motor based on 2D FEM model

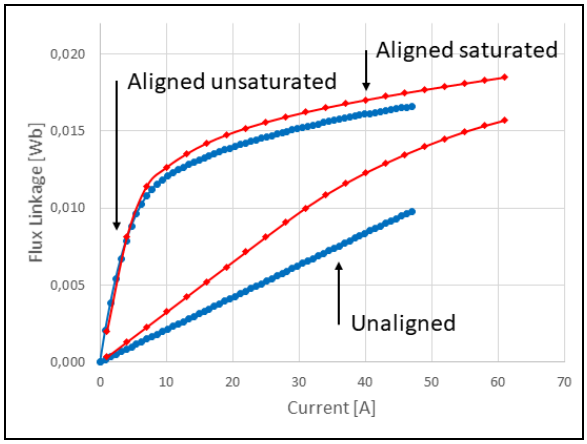

Fig. 3: Comparison of flux calculated using 2D (blue) and 3D (red) models

Another approach is to keep the current flux network, but reduce the losses, which is usually done by reducing the current, as is clear from Eq. (1). To keep the same electrical power, the supply voltage need to increase, which can be achieved by either using a higher rated battery or introducing a step-up converter in the power stage.

In the following sections the four mentioned methods will be described, as well as evaluated with regards to applicability in the research context. Therefore, three criteria are used: performance improvement, potential drone weight change and price.

Flux curve-shaping methods

The two methods allowing the modification of the flux network both deal with modifying the motor design. Saturation level can be increased by changing the stator and rotor material and magnetic flux density can be reduced by simply making the stator teeth wider.

The most suitable candidate in terms of lamination material change seems to be cobalt-iron alloy. In terms of saturation capability, it is rated around 2.3 T, while NO20 steel used in the original design reaches

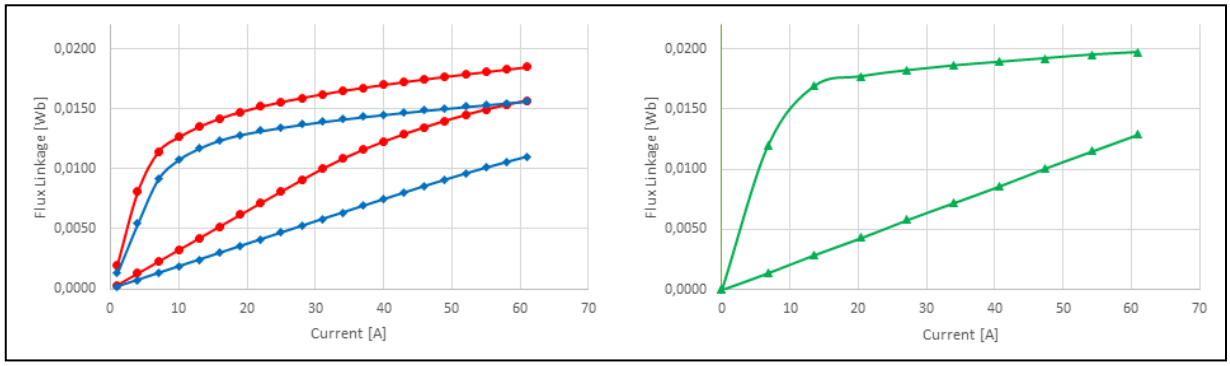

Fig. 4: Comparison of flux networks of original (red), modified (blue) and using cobalt-iron material (green) designs

only up to 1.7 T. Unfortunately, this type of material is significantly more expensive. It is also considerably heavier, with density of 8.12 $^{g}/_{cm^3}$ compared to 7.60 of NO20.

Parameter	*Original design*	*Modified design*
Stator outer diameter [mm]	71.00	71.00
Stator inner diameter [mm]	39.00	40.40
Stator yoke thickness [mm]	3.23	5.50
Stator pole arc	15.00°	20.00°
Stator taper angle	6.75°	3.00°
Rotor outer diameter [mm]	38.60	40.00
Rotor inner diameter [mm]	17.85	17.85
Rotor yoke thickness [mm]	3.06	5.00
Rotor pole arc	16.50°	21.50°
Rotor taper angle	-3.38°	-3.00°
Stack length [mm]	15.00	15.00

Table 2: Differences in geometry between original and modified motor design

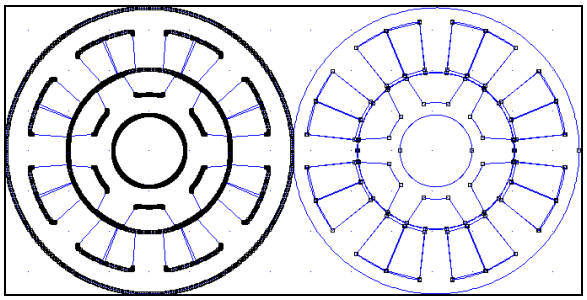

Fig. 5: Comparison of original (right) and modified (left) motor geometry

The problem with any modification of the design is that it needs to be done manually on a trial-and-error basis, as any optimization methodology using 2D models might run into similar problems and 3D models are too computationally expensive. The objective of this adjustment is to bring the 3D model flux network to that of the original design. To this end, while teeth width is the most noticeable change, some minor adjustments were made, such as yoke thickness, airgap length and taper angles. Table 2 and Fig. 5 allow for comparison of original and modified designs.

Another necessary change was to reduce the number of winding turns (while keeping the same fill factor) of the machine from 42 to 30, which was done to better shape the torque-speed curve to the application, as seen in Fig. 6. These modifications have increased the iron weight from 208 g to 271 g, but this is somewhat offset by reduction in copper weight from 103 g to 74 g. In terms of price, the only cost was connected with having to re-simulate the 3D model.

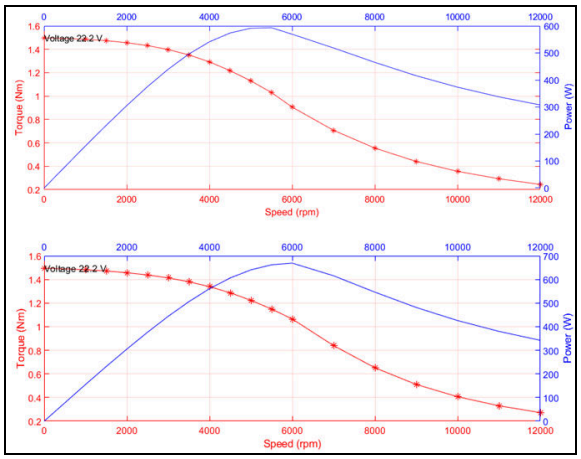

Fig. 6: Comparison of torque-speed characteristic of SR motor with 42- (top) and 30-turn (bottom) winding

The specific impact of these approaches on the flux density is shown in Fig. 4, which compares the original and adjusted designs. Due to technical limitations, only 2D model (computed with FEMM software) was used in the case of cobalt-iron laminations. Therefore, for evaluation purposes, performance including 3D effects estimation is considered.

Voltage-based methods

The UAV chosen as a demonstrator platform was designed to use two 6-cell (6S) Lithium-Polymer (LiPo) batteries, of 12000 mAh capacity each, connected in parallel. That configuration provides from 25.2 V fully charged to 22.2 V when 80% depleted (it is advised against discharging LiPo batteries any further), but this relation is nonlinear. That is why the motor design performance was always evaluated at 22.2 V, to ensure sufficient

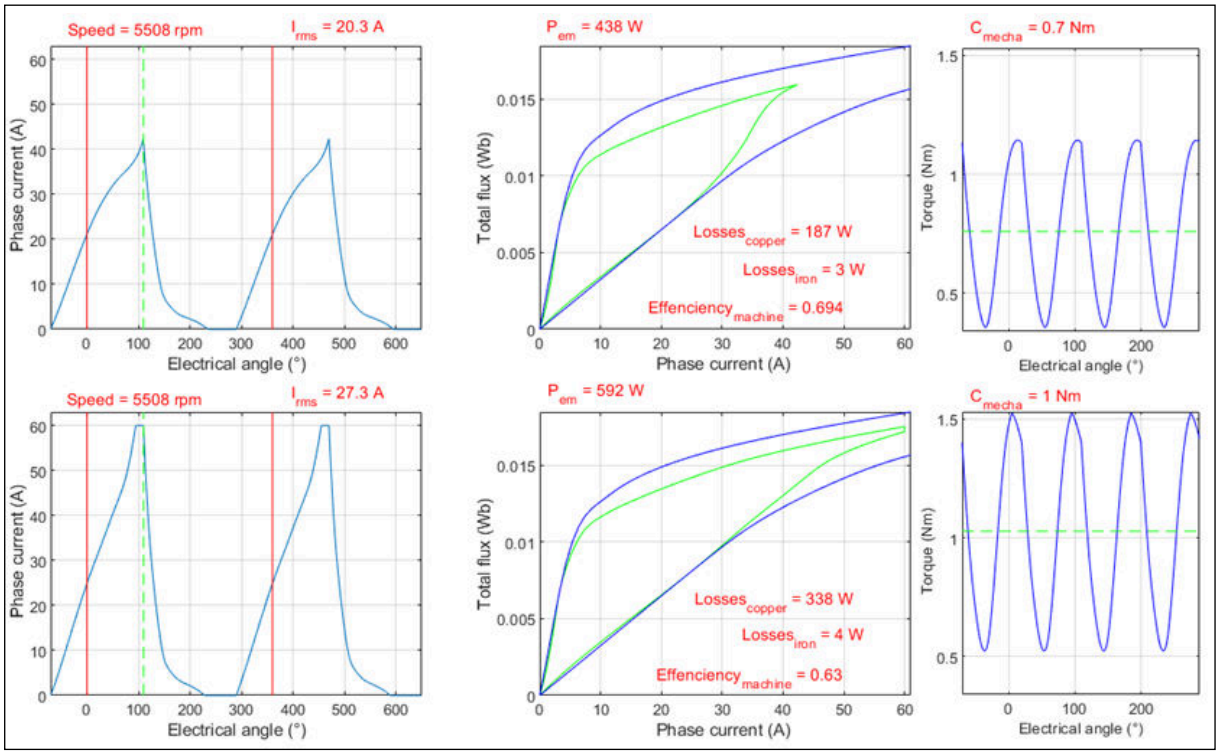

Fig. 7: Motor performance with 6S (top) and 7S (bottom) battery

performance throughout the whole flight, regardless of battery state of charge.

Changing the batteries to a pair of 7S units would result in nominal voltage increase of 3.7 V to 25.9 V (and fully charged voltage to 29.4 V). This would allow more of the flux network area to be utilized, as seen in Fig. 7. However, this is limited by the availability of specific components on the market - for example, the closest 7S battery equivalent has only 10000 mAh capacity, which would severely reduce flight time, but each battery also weights 100 g less, reducing the total weight by 200 g. Unfortunately, this is not enough to offset the drop in available capacity.

The pricing of this approach unfortunately extends beyond simply the cost of the batteries, as supporting electronics, including current sensors and two Battery Elimination Circuits (BECs), need to be upgraded as well. From the maintenance supplies, the charger needs to be changed. Fortunately, both the ESC and BLDC motor of the original drone are able to support up to 8S, so the exchangeability of technologies, allowing for direct comparison, is preserved.

Instead of swapping multiple components of the UAV, it might be possible to achieve a similar effect with a redesigned SR motor power stage. This would require an introduction of a step-up converter, which can be placed either at the battery connection or in each of the four asymmetric bridge converters. This is a hypothetical approach, but for simulation purposes, the second option was chosen, considering easier heat dissipation in a real device. The schematic of a converter for one phase and the associated performance (reduced peak current, increased winding voltage and achieving rated speed) results are shown in Fig. 8.

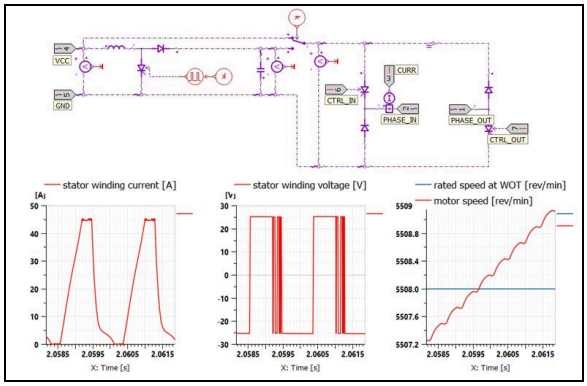

Fig. 8: Schematic and performance (with propeller load) of a step-up circuit incorporated into asymmetric bridge converter (without current limiter)

Due to current limitations, the real application will also require a current limiter to facilitate safe charging of the capacitors, but this will increase the turn-on time of the UAV. However, for the discussed applications this should not be a problem.

It is hard to accurately estimate the weight and price of this solution, as this was not consulted with an external company during that stage of the project. However, price would not be affected much by the cost of the additional components, but design fees (as this is a non-conventional schematic) might be substantial. It is slightly easier to estimate the weight,

as the voltage step is relatively small (3.7 V), so not much additional heatsink area will be needed.

Conclusions

This paper offers a set of solutions to a problem that appears when designing small size SR machines, especially with tight weight constraint. The inductance increase due to end-winding and 3rd dimension flux leakage become a significant obstacle. This problem is related directly to the chosen design process, as flux network computation based on FEM using a 2D motor model is a good balance between time and accuracy, it does not include the phenomena in question. Using 3D models for the whole optimization process is too costly to be considered a viable alternative.

Therefore, the suggested approach is to complete the optimization using 2D models and solve the issues related to 3D effects separately, as a next design step. Two general approaches (with two methods each) are described: 1) to improve the flux network by modifying the motor design and 2) to increase supply voltage. These four methods are evaluated based on not only improvement in performance, but also possible UAV platform weight change and price. The assessment summary can be found in Table 3.

Method	*Performance (compared to 2D model results)*	*Weight*	*Price*
Material change	Minor increase	Minor increase	Major increase
Design modification	Negligible change	Minor increase	Medium increase
Battery change	Minor decrease	Minor decrease	Medium increase
Step-up converter	Minor decrease	Minor increase	Major increase

Table 3: Evaluation of 3D effects mitigation methods

No objective function is provided to make the final selection, as the focus on different aspects is different for every project and it is left to the adopter to make a subjective, but informed, choice. Three of the methods discussed are suitable for safety-critical applications (such as air taxis), as they do not introduce additional points of failure.

References

[1] C. Z. Liaw, W. L. Soong, B. A. Welchko, and N. Ertugrul, “Uncontrolled Generation in Interior Permanent-Magnet Machines,” *IEEE Trans. Ind. Appl.*, vol. 41, no. 4, pp. 945–954, Jul. 2005.

[2] J. M. Miller, “Electric drive system technologies,” in *Propulsion Systems for Hybrid Vehicles*, Institution of Engineering and Technology, 2010, pp. 243–324.

[3] Y. Saadi, R. Sehab, A. Chaibet, M. Boukhnifer, and D. Diallo, “Performance Comparison between Conventional and Robust Control for the Powertrain of an Electric Vehicle Propelled by a Switched Reluctance Machine,” in *2017 IEEE Vehicle Power and Propulsion Conference (VPPC)*, 2017, pp. 1–6.

[4] M. Biczyski, R. Sehab, J. F. Whidborne, G. Krebs, and P. Luk, “Multirotor Sizing Methodology with Flight Time Estimation,” *J. Adv. Transp.*, vol. 2020, pp. 1–14, Jan. 2020.

[5] D. E. Finkel, “DIRECT Optimization Algorithm User Guide.” p. 14, 2003.

[6] A. Kolli, G. Krebs, X. Mininger, and C. Marchand, “Impact of command parameters on efficiency, torque ripple and vibrations for Switched Reluctance motor,” in *2012 XXth International Conference on Electrical Machines*, 2012, pp. 2975–2980.

[7] M. Tursini, M. Villani, G. Fabri, and L. Di Leonardo, “A switched-reluctance motor for aerospace application: Design, analysis and results,” *Electr. Power Syst. Res.*, vol. 142, pp. 74–83, Jan. 2017.

[8] T. J. E. Miller, *Electronic Control of Switched Reluctance Machines*. Elsevier, 2001.

Designing low-weight switched reluctance motors for electric multirotor propulsion system

Biczyski, Marcin

2021-10-21

Biczyski M, Sehab R, Krebs G, Whidborne J & Luk P (2021) Designing low-weight switched reluctance motors for electric multirotor propulsion system. In: MEA 2021 More Electric Aircraft, 20-21 October 2021, Bordeaux, France, P2-20

https://see.asso.fr/369398_mea2021-proceedings/